Characterization of Liquid-Liquid Dispersions with Variable Viscosity by Coupled Computational Fluid Dynamics and Population Balances

Michal Vonka and Miroslav Soos
Dept. of Chemistry and Applied Biosciences, Inst. for Chemical and Bioengineering, ETH Zurich, 8093 Zurich, Switzerland

Dept. of Chemical Engineering, University of Chemistry and Technology, Technicka 5, 166 28 Prague, Czech Republic

DOI 10.1002/aic.14831
Published online April 23, 2015 in Wiley Online Library (wileyonlinelibrary.com)

Sustaining stable liquid-liquid dispersion with the desired drop size still relies on experimental correlations, which do not reflect our understanding of the underlying physics and have a limited prediction capability. The complex behavior of liquid-liquid dispersions inside a stirred tank, which is equipped with a Rushton turbine, was characterized by a combination of computational fluid dynamics and population balance equations (PBE). PBE took into account both the drop coalescence and breakup. With the increasing drop viscosity, the resistance to drop breakage also increases, which was introduced by the local criteria for drop breakup in the form of the local critical Webber number (We_c*). The dependency of* We_c *on the drop viscosity was derived from the experimental data available in the literature. Predictions of Sauter mean diameter agree well with the experimentally measured values allowing prediction of mean drop size as a function of variable viscosity, interfacial tension, and stirring speed.* © 2015 American Institute of Chemical Engineers *AIChE J*, 61: 2403–2414, 2015

Keywords: liquid-liquid dispersion, turbulent flow, breakup, coalescence, variable viscosity effect, interfacial tension effect

Introduction

Dispersion processes are frequently used in industry to increase the heat removal and to provide large interfacial area available for mass transfer. However, maintaining stable dispersions with the desired drop size distribution (DSD) in large industrial tanks still poses a difficult task with high economic risks involved. To control and optimize the dispersion processes in agitated vessels, both the coalescence and breakup processes have to be taken into consideration. For the coalescence, the key factors are the collision frequency between two colliding drops, time of their contact, and mobility of the drop surface. The drop breakup is determined by the balance between the disrupting forces and the cohesive forces. The disrupting forces are induced by the flow, which is typically turbulent, while the cohesive may be twofold: the interfacial tension that keeps the drop spherical, and the internal viscose resistance.

Due to the complex nature of the dispersion processes, there are many correlations between the mean or maximum stable drop size and the global process parameters.[1] The correlations are usually expressed in terms of the dimensionless numbers, one of which is the tank Weber number[2] defined as

$$We_{\mathrm{T}} = \rho N^2 D_{\mathrm{imp}}^3 / \sigma \tag{1}$$

with ρ referring to the density of the continuous phase, N is the mixing frequency of the impeller, and D_{imp} is its diameter. The other group, introduced to capture the dependency of stable drop size on the dispersed-phase viscosity, is the viscosity group defined as[2]

$$\mathrm{Vi} = \mu_{\mathrm{d}} / \sqrt{\rho_{\mathrm{d}} \sigma} \tag{2}$$

where μ_{d} and ρ_{d} refers to the viscosity and density of the dispersed phase, respectively, and σ is the interfacial tension, which is a strong function of the type and amount of used surfactant. Despite the practical usefulness of these empirical correlations, they also have several drawbacks. From scientific point of view, the most important is the omission of the details of the physics involved in the governing mechanisms. On the other hand, the narrow applicability window of operating conditions, for which, these correlations were determined, poses a strong limitation for the engineering applications. Bearing all these limitations, the correlations between dimensionless groups cannot predict conditions, that is, interfacial tension, viscosity, mixing rate, or vessel geometry, which are outside the range of the experimental data used for their derivation. Also, recent knowledge presented by several authors who studied breakup of drops or fractal aggregates in stirred tanks[1,3] or in an axisymmetric extensional flow,[4–6] indicates that particularly breakage is

Corresponding concerning this article should be addressed to M. Soos: at miroslav.soos@vscht.cz or miroslav.soos@chem.ethz.ch

controlled by the local hydrodynamic properties rather than the global characteristics.

In a stirred tank, an efficient way to investigate the details of the fluid flow and its impact on the coalescence and breakup processes is the combination of multiphase flow model with the model of coalescence and breakup. The flow can be modelled by the computational fluid dynamics (CFD) while the dispersion processes are captured by population balance equations (PBE). In the past, successful applications of this combined approach for gas-liquid dispersions have been presented by several researchers.[7–18] As concluded in these works, the modelling of the dispersed systems requires a careful choice of the coalescence and breakage rate expressions, also called kernels. A comprehensive comparison of available coalescence and breakage kernels for the gas-liquid and liquid-liquid systems can be found in the reviews of Liao and Lucas.[19,20] More consensus has been reached among scientist, in the case of the coalescence kernel, while the breakup kernels exist in various forms in the literature.[20] Depending on the choice of the kernel, there could be several adjustable parameters, which are commonly obtained by fitting of the model against a suitable set of experimental data. Obviously, models with lower number of adjustable parameters are preferred. One of them is the criteria for bubble/drop breakup. This is commonly provided in the form of the local value of the Weber number defined as[2]

$$We_c = \tau L/\sigma \tag{3}$$

with τ being the stress imposed by the fluid on the surface of the bubble/drop and L representing the bubble/drop size. Since the size of bubbles/drops is commonly larger that the Kolmogorov microscale $\left(\eta_k = (\nu^3/\varepsilon)^{1/4}\right)$ their breakup occurs in the inertial subrange of turbulence. Together with the assumption of the isotropic turbulence,[21] this leads to an approximation of the hydrodynamic stress in Eq. 3 as

$$\tau = \frac{1}{2}\rho\,\langle \Delta u^2(d)\rangle \tag{4}$$

where $\langle \Delta u^2(d)\rangle$ is the mean square difference in the velocity between two points separated by the distance d, sometimes referred to as the second-order velocity structure function.[21,22] In the case of the inertial subrange of turbulence, the mean square difference in velocity takes the form of

$$\langle \Delta u^2(d)\rangle = C_3(\varepsilon d)^{2/3} \tag{5}$$

where ε is the local energy dissipation rate and C_3 is a constant, which under the assumption of the isotropic turbulence is around two.[21,23] Combining Eqs. 3–5, and assuming that the separation distance d is comparable to the diameter of the bubble/drop, we arrive to the expression of the breakup criterion

$$We_c = \rho\,\varepsilon^{2/3} L^{5/3}/\sigma \tag{6}$$

For the modelling of the dispersion processes by a combination of CFD and PBE Eq. 6 is preferred to Eq. 1 due to the direct relation between the local values of ε, size of the bubbles or drops, and the interfacial tension. In the case of air bubbles in water, We_c is commonly assumed to be equal to 2.3 (see, e.g., Prince and Blanche[24] or Venneker et al.[7]) with no dependency on the dispersed-phase viscosity. However, liquid-liquid dispersions exhibit a strong effect of the dispersed-phase viscosity on the maximum stable drop size[25] as well as breakup mechanism[26] which indicates no unique value of We_c.

In recent work, Becker et al.[27] studied the breakage of drops with variable viscosity in the presence of the surface agent and also reported increasing resistance to breakage with the increasing drop viscosity. They proposed a modification of the breakup kernel originally derived by Luo and Svendsen[28] by an additional term related to the internal resistance of the drop imposed by the viscosity. Model validation was performed for various oils with viscosity between 0.02 and 0.35 Pa s and the dispersion was stabilised by a fast-acting surfactant. The stabilization resulted in similar interfacial tension in the studied systems. Although the breakup model seems promising, some controversy remains about the drop size below the inertial subrange and the eddy size which breaks the drop, which is assumed substantially larger than the breaking drop size (approximately two orders of magnitude). These conclusions are not in agreement with previous literature studies, where the maximum size of the breaking eddies was reported between the size of the drop and 10× the drop size. Larger eddies are deemed responsible for the drop transport rather than for their breakup.[24,26] The same group applied the modified breakup kernel for a CFD analysis of a high-pressure homogenizer.[29]

Combined CFD-PBE models offer an efficient tool for inspection of the turbulent behavior of liquid-liquid dispersions, and such modelling extends the knowledge beyond the correlations of nondimensional groups. However, predictions of behavior outside fitting bounds are scarce and even CFD-PBE coupled models have not yet extended for predictions of the variable geometries, holdups of the dispersed phase, viscosities of both phases, or interfacial tension.

To predict the dispersion characteristics at variable conditions, i.e. the dispersed phase viscosity, interfacial tension, mixing rate, we formulated a CFD-PBE model which was validated against the experimental data of Wang at al.[30] From these data, we formulated a local breakup criterion in the terms of the critical Weber number We_c described by Eq. 6. Figure 1 shows an example of the We_c calculated from experimental data,[30] measured in a stirred tank which was equipped with six-blade Rushton turbine. The impeller was in the center of the vessel equipped with four baffles that had the width equal to the 1/10 of tank diameter. A very broad range of the dispersed-phase viscosities and interfacial tensions covering range from 0.001 Pa s up to 1 Pa s, and from 0.045 N/m down to 0.007 N/m, respectively, was investigated by Wang and Calabrese.[30] Since these data were measured for a low volume fraction of the dispersed phase equal to 0.15%, the coalescence was substantially suppressed and the breakup was assumed as the dominant mechanism which controlled the size of formed drops. The operation in the breakage dominant region implies that the size of maximum stable drops was determined by the maximum value of the energy dissipation rate present in the system, ε_{max}.[1,4] Even though the used configuration of the stirred tank is frequently studied in the literature, the reported values of ε_{max} vary significantly.[1,3,31–36] To avoid any *a priori* choice of ε_{max} and considering that all presented data of Wang and Calabrese[30] were measured using the same vessel operated at the same stirring speed, we show the values of We_c normalized with respect to the lowest viscosity of dispersed phase, that is, 0.001 Pa s.

As can be seen from Figure 1, the measured data follow closely the same trend although it was obtained at variable interfacial tension, σ, between the phases, which in the

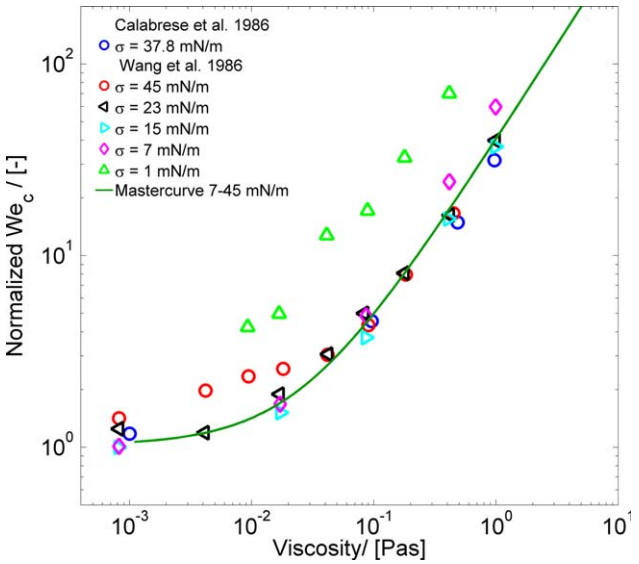

Figure 1. Data of Wang and Calabrese[30] measured for different viscosity of the dispersed phase and various values of the interfacial tension replotted in terms of critical Weber number (We_c) which was normalized by We_c obtained for viscosity of the dispersed phase equal to 0.001 Pa s.

[Color figure can be viewed in the online issue, which is available at wileyonlinelibrary.com.]

ranged from 0.007 to 0.0378 N/m. The change of σ was obtained using pure water or mixture of water and methanol as the continuous phase. Such reduction of σ did not cause any steric stabilization of droplets as it would be by surfactant addition. For the case of the pure methanol as continuous phase, which corresponds to the lowest interfacial tension, a deviation from the waterborne curve is observed. This indicates that for waterborne systems the interaction between the continuous phase and the silicone oil is different compare to the system of silicone oil dispersed in pure methanol. The reasons may be twofold: (1) change in molecular interaction due to different amount of hydrogen bonds and/or (2) higher solubility of the methanol in the silicone oil.

We assumed that dependency of the measured stable drop size on interfacial tension for waterborne systems is properly captured by We_c, which corresponds to data in Figure 1. In contrast to the interfacial tension effect, We_c is not capable of capturing the dependency of the maximum stable drop size on the dispersed-phase viscosity. First, reported by Hinze,[2] this phenomenon lead to the introduction of the viscosity group (Eq. 2). Since the CFD-PBE cannot locally solve the usually nonlinear correlation between the viscosity group and Weber number (Calabrese et al.[25]), we proposed a viscosity-dependent We_c (see line in Figure 1). This allows us to incorporate an additional contribution of the drop viscosity to the breakup resistance and serve as a local breakup criterion. The obtained dependency of We_c on the dispersed-phase viscosity is linear, which is the same form as the kernel modification proposed by Becker et al.[27] The obtained We_c was consequently used to study the effects of dispersed-phase viscosity, interfacial tension, and stirring speed on the mean stable drop size in diluted dispersions without presence of surfactant where both coalescence and breakup took place. The study was conducted by a combination of CFD multiphase model of whole vessel combined with the PBE. The geometry represented the stirred vessel used by Calabrese and coworkers.[25,30,37]

The data of Wang and Calabrese[30] were collected for constant stirring speed, the predictive power of the proposed model was tested using another dataset generated by the same group.[25] This dataset reports the mean stable drop size as a function of the applied stirring speed and viscosity of the dispersed phase in water media, while using a self-similar mixed vessels of various sizes equipped with the Rushton turbine. Furthermore, to cover also the dispersed-phase viscosity of 0.001 Pa s, incorporated the data of Chen and Middleman,[38] which also describe the mean drop size at variable mixing speeds.

Model Formulation

Hydrodynamic model

For modelling of a dilute dispersion, the Euler-Euler approach gives a good approximation of the liquid-liquid multiphase system.[39–41] This concept consists of solving of the continuity equation and momentum balance equation for each phase. In this formulation, the continuity equation of each phase has form

$$\frac{\partial}{\partial t}(\phi_k \rho_k)+\nabla\cdot(\phi_k \rho_k \bar{\mathbf{U}}_k)=0 \tag{7}$$

where ϕ, ρ, and $\bar{\mathbf{U}}$ are volume fraction, density, and velocity vector. Lower case index k refers to the continuous (c) or dispersed (d) phase, respectively. To obtain $\bar{\mathbf{U}}$, one needs to solve the momentum conservation equation

$$\frac{\partial}{\partial t}(\phi_k \rho_k \bar{\mathbf{U}}_k)+\nabla\cdot(\phi_k \rho_k \bar{\mathbf{U}}_k \bar{\mathbf{U}}_k)=-\phi_k \nabla p +\nabla\cdot\mathbf{T}_k+\mathbf{F}_{drag}+\phi_k \rho_k g \tag{8}$$

where ∇p, $\mathbf{T}$, $\mathbf{g}$, and $\mathbf{F}_{drag}$ represent the pressure gradient, total stress tensor, gravity acceleration, and drag force, respectively. The sign of the drag force is considered negative for the dispersed phase and positive for the continuous phase. The turbulent term in the momentum balances (Eq. 8) was resolved by the standard $k-\varepsilon$ model, where the turbulent kinetic energy, k, and the energy dissipation rate, ε, are obtained by solving additional two conservation equations defined as follows[21]

$$\frac{\partial}{\partial t}(\rho_m k)+\nabla\cdot(\rho_m k \bar{\mathbf{U}}_m)=\nabla\cdot\left(\frac{\eta_t}{\sigma_k}\nabla k\right)+G_k-\rho_m \varepsilon \tag{9}$$

$$\frac{\partial}{\partial t}(\rho_m \varepsilon)+\nabla\cdot(\rho_m \varepsilon \bar{\mathbf{U}}_m)=\nabla\cdot\left(\frac{\eta_t}{\sigma_\varepsilon}\nabla \varepsilon\right)+\frac{\varepsilon}{k}(C_1 G_k - C_2 \rho_m \varepsilon) \tag{10}$$

where η_t is turbulent viscosity. σ_k, σ_ε, C_1, and C_2 are model constants. Lower case index m denotes mixture of phases. G_k represents the production of the turbulent kinetic energy given by

$$G_k=-\rho\left(\nabla\bar{\mathbf{U}}_c(\nabla\bar{\mathbf{U}}_d)^T\right)\nabla\bar{\mathbf{U}}_d \tag{11}$$

The turbulent viscosity is given by equation

$$\eta_t=C_\eta \rho\frac{k^2}{\varepsilon} \tag{12}$$

where C_η is a hydrodynamic constant.[21]

Population balance modelling

To model the behavior of dispersion without the surface agent, we used the coalescence and breakup of the dispersed drops, which formed the respective terms of the PBE.[42] Even though experiments of Wang and Calabrese[30] and Calabrese et al.[25] were performed at the low volume fraction of the dispersed phase, that is, in the breakage dominant conditions, the coalescence cannot be completely neglected if the model should represent the processes in the vessel at variable process conditions. As reported by Zhou and Kresta,[32] the smallest drops generated by breakage of the mother drops can have size below the Kolmogorov length scale. For low viscosities of the dispersed phase these drops are prone to coalescence even in diluted systems if the mixing speed mixing is sufficient.[1] According to these findings we considered the general form of PBE consisting of breakage and coalescence, while we neglected the drop growth or diffusion terms has a form

$$\frac{\partial n(L_i)}{\partial t}+\nabla\cdot(\bar{\mathbf{U}}_d\, n(L_i))=B^B(L_i)+B^C(L_i)-D^B(L_i)-D^C(L_i) \tag{13}$$

where $n(L_i)$ represents the number density function of drop with size L_i. B and D are the birth and death terms due to coalescence and breakage, respectively, as indicated by the corresponding upper index. $n(L_i)$ is also a function of time and space,[43–45] but for the sake of simplicity full notation of coordinates is omitted.

Let us now discus the respective terms of PBE. Birth by breakage is usually assumed as a source term related to the probability that a larger drop with size L_j will break into a smaller size L_i. This can be expressed as

$$B^B(L_i)=\int_{L_i}^{\infty}\beta(L_i,L_j)g(L_j)n(L_j)dL_j \tag{14}$$

where $\beta(L_i,L_j)$ is the daughter distribution function (DDF), $g(L_j)$ is the breakage kernel, $n(L_j)$ represents number density function of drops larger than L_i, which can break into this size. Drops of size L_i can break into smaller drops, which happens with rate $g(L_i)$ and the resulting death source term is

$$D^B(L_i)=g(L_i)n(L_i) \tag{15}$$

Smaller drops coalesce into the drops of size L_i with rate $h((L_i^3-L_j^3),L_j)$. The overall source term can be written as

$$B^C(L_i)=\frac{1}{2}\int_0^{L_i}h((L_i^3-L_j^3),L_j)n((L_i^3-L_j^3)^{1/3})n(L_j)dL_j \tag{16}$$

Drop of size L_i may also coalesce with an arbitrary drop, which results in a death source term, which has a shape

$$D^C(L_i)=\int_0^{\infty}h(L_i,L_j)n(L_i)n(L_j)dL_j \tag{17}$$

Coalescence Frequency. The coalescence kernel $h(L_i,L_j)$ was assumed as a product of the drop interaction frequency, ω^C, and the efficiency of such an interaction, p^C. A phenomenological model of coalescence frequency is based on the concept of a moving drop, which interacts with other drops along its pathway. In analogy to the kinetic theory of gases[46] and with the assumption of (1) the isotropic turbulence around the colliding drop, and (2) the drop sizes in the inertial subrange, it is possible to derive the interaction frequency of drops in turbulent flows.[24] For more details, see the original work of Prince and Blanch.[24] When considering the statistical turbulent velocity of a drop in a form of Eq. 5, the collision rate can be expressed as[24]

$$\omega^C(L_i,L_j)=\frac{\sqrt{2}\pi}{16}\varepsilon^{1/3}(L_i+L_j)^2\sqrt{L_i^{2/3}+L_j^{2/3}} \tag{18}$$

Note that even though Eq. 18 represents the original idea of the gas kinetic theory, various formulations are presented in the literature.[7,19]

Coalescence Efficiency. Whether colliding drops will undergo coalesce or not is controlled by the time required for the coalescence and the time available for.[47] According to the standard mechanism of coalescence, the time required for coalescence is related to the time required to drain the liquid trapped in the thin film at the deformed drop-drop interface. Following the work of Prince and Blanch,[24] the efficiency of collision, p_C, was formulated as the exponential of the ratio of the critical time, t_{Cr}, necessary for coalescence and the contact time available, t_{Co}, computed with respect to flow conditions. The collision efficiency takes form of

$$p^C(L_1,L_2)=\exp\left[-\frac{t_{Co}}{t_{Cr}}\right] \tag{19}$$

Since viscosity has a strong effect on the interface mobility, t_{Cr}, was expressed as a contact time of two semimobile interfaces according to Harrats[48]

$$t_{Cr}=\frac{\sqrt{3}\eta_d\eta_c^{1/2}\dot{\gamma}^{1/2}R^{5/2}}{4\sigma^{3/2}}\left(\frac{1}{h_{Cr}}-\frac{1}{h_0}\right) \tag{20}$$

where $\dot{\gamma}$, R, h_c, and h_0 represent the shear rate, equivalent radius of collision, critical, and initial separation distances of surfaces, respectively. The critical distance, where the rupture of the trapped film occurs, was approximated by formulation of Chesters[49]

$$h_{Cr}=\left(\frac{HR}{8\pi\sigma}\right)^{1/3} \tag{21}$$

where H is Hamaker constant in the case of systems with high viscosity of the dispersed phase, the initial separation distance, h_0, is usually very small compared to h_{Cr}, thus, it was neglected.

An additional quantity required to calculate the critical time of coalescence in Eq. 20, is the shear rate, $\dot{\gamma}$. Assuming isotropic turbulence $\dot{\gamma}$ can be related to the energy dissipation rate and fluid properties by equation

$$\dot{\gamma}=\sqrt{\frac{\varepsilon\rho_c}{\eta_c}} \tag{22}$$

Equivalent radius of colliding drops was defined as

$$R=\frac{L_iL_j}{L_i+L_j} \tag{23}$$

According to Levich and Kuznetsov,[50] the contact time in turbulent flow which expresses the available time for two drops to coalesce was estimated as

$$t_{Co} \approx \frac{(L_1+L_2)^{2/3}}{\varepsilon^{1/3}} \tag{24}$$

Breakage Frequency. In the oil-water system, where the components have very similar densities, the drops can break either due to turbulent shear stresses or contact with the vessel instrumentation. Since the density of continuous and dispersed phase[25,30] was comparable, it was assumed that drops follow closely the flow. Under such conditions, the drop breakup can occur only due to the local hydrodynamic stresses originating from the turbulence, that is, when the drop hits an eddy which contains sufficient energy to break it.

According to Kolmogorov energy cascade theory,[22] multiple eddies of various sizes and energies are present in the turbulent flow at one place, therefore, it is advantageous to inspect the eddies of various sizes and their possibility to break the given drop.[7,28] Consequently, the breakage rate can be assumed as an integral of all relevant eddies

$$g(L) = \int_{\lambda_{min}}^{\lambda_{max}} \omega^B(L,\lambda) p^B(L,\lambda) d\lambda \tag{25}$$

where λ is the length of an eddy, $\omega^B(L,\lambda)$ is the frequency of drop interaction with eddies and $p_b(L,\lambda)$ is the breakage efficiency. Both eddy minimum and maximum sizes, which must be taken into account, are often discussed in the literature.[7,24,51] As shown by Andersson and Andersson,[26] boundaries of integral in Eq. 25, has strong impact on the breakup process. Following their theoretical findings, the lower bound of the eddy size, λ_{min}, was chosen to be one-tenth of the drop size. Due to the nature of the breakage kernel, the impact of selection of λ_{min} was very small. Conversely, the choice of upper bound of the eddy size, λ_{max}, has a strong impact on the breakup kernel. Values of λ_{max} from the drop size up to 10 times, the drop size were used for the modelling the drop breakup.[7,45,51] An exception is a recent work of Becker et al.[27] who suggested that λ_{max} should be in the order of 100 times of the drop. In our work, λ_{max} was set to be equal to the drop diameter while it was assumed that larger eddies will transport the drop.[26]

Collision frequency is dependent on the size of the colliding drops (L) and eddies (λ), that are present in the turbulent flow during the breakage event. Following the previous works, which described the breakup of bubbles in turbulent flow,[7,24,28] we assumed the resulting collision frequency in the form

$$\omega^B(L,\lambda) = \frac{\sqrt{2}\pi}{16} \varepsilon^{1/3} (L+\lambda)^2 \sqrt{L^{2/3}+\lambda^{2/3}}\, n_\lambda \tag{26}$$

where n_λ is the number density probability of an eddy with a given size. Under the assumption that the drop breakup occurs in the inertial subrange of turbulence, n_λ can be estimated from the turbulent energy spectra as follows[7,28]

$$n_\lambda = \frac{12(1-\phi)}{\pi \lambda^4} \tag{27}$$

Breakage Efficiency. Many formulations of breakage efficiencies are present in literature.[20] The most common formulation is based on the balance of the critical energy necessary for the drop breakup, being proportional to u_{cr}, and the energy brought by an eddy, being proportional to u_λ, defined as follows[20]

$$p^B(d,\lambda) = \exp\left[-\frac{u_{cr}^2}{u_\lambda^2}\right] \tag{28}$$

The energy of the eddy per unit mass can be calculated according to Eq. 5 by substitution of eddy size λ instead of drop size L_i. When considering definition of the local Weber number (Eq. 3), the critical energy of collision was defined as

$$u_{Cr}^2 = \frac{We_c \sigma}{\rho_c L} \tag{29}$$

It was shown[1,4] that the maximum size of a drop or fractal aggregate, which was measured at steady state, is controlled by the value of maximum energy dissipation rate present in the system. To obtain We_c as a function of viscosity (see Figure 1 and Eq. 6), it is necessary to determine the maximum steady state drop size, L_{max}, which can survive in the given flow described by the corresponding maximum energy dissipation rate ε_{max} that the drop can withstand before breakage. In our case, L_{max} was obtained from the relation $L_{32} = C_5 L_{max}$, proposed by Sprow,[52] with L_{32} referring to the Sauter mean drop size. The parameter C_5 depends on the dispersed-phase viscosity and applied stress. Reported values in the open literature vary from 0.38 to 0.69.[1] In our case, the C_5 was adopted from the experiments of Calabrese et al.[25] The breakage resistance of the drop, expressed in terms of the maximum energy dissipation rate ε_{max}, was obtained by fitting of the results calculated by the CFD-PBE model against the experimental data of Wang et al.[30]

Daughter Distribution Function. The drop breakage occurs by various mechanisms according to the fluid stresses, drop viscosity, and interfacial tension. A comprehensive study of breakup mechanisms in Andersson and Andersson[26] suggests that macroscale surface perturbations lead to breakage of liquid drops into multiple similar-sized fragments for low and moderate viscosities of dispersed phase. In such case symmetric breakage assumption is considered reasonable for the liquid-liquid systems, since the breakage event results in two or three larger daughter drops of similar size and a few small satellite drops with negligible volume fraction of the mother drop. At higher viscosities, the dispersed phase under elevated stress forms liquid threads which break into multiple fragments of unequal size. We used the DDF reported in Laakkonen et al.[8] in the form of a beta distribution

$$\beta = \left(9 + \frac{33}{2}C_4 + 9C_4^2 + \frac{3}{2}C_4^3\right)\left(\frac{L_i^2}{L_j^3}\right)\left(\frac{L_i^3}{L_j^3}\right)^2\left(1-\frac{L_i^3}{L_j^3}\right)^{C_4} \tag{30}$$

where C_4 is a parameter determining the shape of the distribution. Laakkonen et al.[8] adjusted the value of C_4 against experimental data, while others[45,53,54] assigned the value of C_4 according to the mechanism of breakup. In this work, we used ternary breakage mechanism into comparable size fragments, however, the effect of C_4 on the final drop size was tested as well.

Drag coefficient Coupling. The PBE supplements us with the size of the drops, which together with the drag coefficient of dispersed phase C_D give the drag force of drops imposed on the fluid.[55] Various forms of drag coefficient are available in literature.[56,57] In this work, the form proposed

by Morsi and Alexander[58] which is suitable for liquid-liquid systems was used

$$C_D = a_1 + \frac{a_2}{Re_P} + \frac{a_3}{Re_P^2} \quad (31)$$

where $Re_P = \rho_C \bar{U}_m L/\eta_C$ is the Reynolds number for a spherical particle and a_{1-3} are constants adopted from Morsi and Alexander.[58]

Numerical Approach. We modelled the tank of a standard geometry with a Rushton turbine which was used by Calabrese.[25,30,37] Although they used four vessels of different size, their geometrical ratios were held constant. This geometrical similarity results in the identical scaling of the drop size with the tip-speed of the impeller, therefore, we modelled only the smallest vessel with a diameter $T = 0.142$ m. The impeller width and the its clearance was equal to $T/2$ and the baffle size was $T/10$.

The vessel was drawn and meshed in Gambit software. We used a mesh with 14 elements along the impeller blade height and 18 elements along the blade width. The total number of elements in the symmetric half of the stirred tank was equal to 198,943. The minimal orthogonal quality was 0.835, the maximal aspect ratio was 4.6 and the maximal y^+ was 33. To reduce the computational cost of the simulation, the rotation of the zone around the impeller was modelled by the moving reference frame (MFR) method. Second-order upwind discretization was used for all simulations. The pressure-velocity coupling was solved using "Coupled" algorithm. For the modelling of the diluted system, we used the Euler-Euler multiphase model. The oil-phase content was very low, $\phi_{OIL} = 0.0015$, which was chosen according to the experimental work.[30,37] The CFD simulations were conducted in the commercial code Ansys Fluent 14.0.

To verify that simulation results were not mesh-dependent, we carried out two mesh refinements. The first refinement was carried out with respect to the gradient of ε, which is convenient for PBE as all the kernels were based on the flow conditions characterized by ε. The grid was refined at places with high turbulence, that is, 97% of the refinement was in the impeller area. The original mesh of 198,943 cells expanded to 232,109 cells. Because the refinement with respect to gradient of ε was aimed mostly at the impeller region, another refinement of the original mesh was carried out with respect to the velocity gradient. The mesh was refined to 316,803 cells through the whole vessel. Calculated flow conditions and the drop size distribution (DSD) from the original and two refined meshes are compared in the Results section.

The solution of PBE was realized by a User Defined Function written in C++ programing language. The six additional transport equations were solved to track six moments of the DSD during the simulation. With moments of distribution as user defined scalars, the ANSYS Fluent can compute their material derivative, while the user supplements the source terms, that is, the right-hand side of PBE, see Eq. 13.

To solve PBEs, we used the quadrature method of moments (QMOM), which requires numerical procedures such as the product difference algorithm[59] and algorithms for overcoming the moment corruption, all of which was adopted from Petitti et al.[45] Solution of the integral in Eq. 25 requires a numerical integration which must be sufficiently simple, fast, and accurate to integrate in each cell of the computational grid. We choose the rectangle rule for its simple implementation, little requirements for allocated memory and no need of *a priori* knowledge of the shape of the integrated function. Number of rectangles varied between 50 and 100, which was adjusted to obtain results with error lower than 5% compared to advanced numerical techniques.[26,60] Integration of Eq. 30 was carried out by Gauss-Legendre rule with seven nodes. Precision of this integration method is discussed in Petitti et al.,[45] and the method is advantageous for the computational speed in case where the shape of the integrated function is known in advance.

Two-way coupling between solution of the flow field and PBE was used in this work, in every discrete volume of the mesh as follows. The solution of PBE was affected by the flow conditions given by ε and, while the flow was adjusted by the drag force computed according to the local drop size and ϕ_D. Specifically, the Euler-Euler model of multiphase flow was initially calculated with a constant drop diameter (1 mm). On this flow pattern, PBE model was computed and new drop sizes at every position of the vessel were obtained. Once DSD was calculated, the drag coefficient was supplemented with the local Sauter mean diameter and a new flow field computation was performed. Subsequent iteration between CFD and PBE computations was conducted until a steady state was reached. Diluted systems converge very fast through these iterations and only up to two iterations were required.

We carried out the simulation on a machine with 32 cores and used the possibilities for process parallelization. The cores operate at frequency 2.7 GHz and the overall RAM was 64 GB. On this machine, the computation of flow on the original grid took around 2 h and iterations were carried out until the scaled residuals became less than 10^{-5}, which usually requires up to 2000 iterations. Solving PBE requires far more iterations, around 15,000, and took around 8 h to reach the same precision. Note that in the case of the flow computation, 12 variables in each cell were solved, while the PBE requires tracking of only six moments. With a good initial guess, the solution is reached fast, therefore, switching between flow and PBE computation requires far less time to converge after the first solution is found.

Results and Discussion

Flow characterization

The tank used by Calabrese and coworkers[25,30,37] to experimentally measure drop breakup was characterized by the CFD techniques with the multiphase dispersion described by the Euler-Euler model. The impeller was a six-blade Rushton turbine, and the vessel was equipped with four baffles. In this section, we report basic flow characterization in terms of the tip speed, v_{tip}, torque, *To*, power number, *Po*, maximum and mean energy dissipation rate, ε_{max}^{Flow} and $\langle\varepsilon\rangle$, respectively, all of which are listed in Table 1 for mixing frequencies from 110 to 330 rpm with water media inside the tank.

Both ε_{max}^{Flow} and $\langle\varepsilon\rangle$ are computed from turbulent fluctuations, which is a widely used approach in literature.[7,45] Note that ε_{max}^{Flow} characterizes the flow conditions together with the used mesh, which is different from the drop breakup resistance, abbreviated as ε_{max}.

There are two ways to obtain *Po*. One is to average the values of ε through the whole vessel, and the other is to calculate *To*, that is, momentum imposed on the impeller by the

Table 1. Flow Conditions Inside the Tank

RPM	v_{tip}	Re_{tank}	To	Po	$\varepsilon_{max}^{Flow}/\langle\varepsilon\rangle$
110	0.41	10,353	0.0039	4.1	114
180	0.67	16,941	0.0125	4.4	118
330	1.23	31,059	0.0371	4.3	119

fluid. For all mixing speed, the ratio between $\langle\varepsilon\rangle$ from To and from averaging of local ε through the vessel is around 1.1, which indicates mesh describing the flow adequately without any significant over- or under-prediction of ε. The Power number obtained from To ranged from 4 to 4.4 with an increasing trend as Re_{tank} increases. Comparable values were reported by Rutherford et al.[61] as well as Joshi et al.[62] for comparable Re_{tank}. Conversely, increasing trend indicates that the flow was not yet fully turbulent, where the Po between 5 and 5.5 is commonly reported using Re_{tank} above 40,000.[61,63–65,73] Based on this, we can conclude that our mesh, the $k-\varepsilon$ model and MFR technique represents the flow adequately. We are well aware, that the validity of the $k-\varepsilon$ model for certain part of turbulent flow, that is, trailing vortexes, is not sufficient,[66,67] however, combination of CFD and PBE complicates application of more precise turbulent models.[72]

As can be seen from Figure 2a, the distribution of ε in the studied stirred tank is very heterogeneous covering approximately four orders of magnitude with $\langle\varepsilon\rangle=0.083$ m^2/s^3 and $\varepsilon_{max}^{Flow}=9.8$ m^2/s^3. During the ε-based mesh refinement, To dropped slightly and maximum energy dissipation rate increased $\varepsilon_{max}^{Flow}=25.9$, which corresponds to 290 $\langle\varepsilon\rangle$. The flow conditions on the mesh obtained from the velocity gradient mesh refinement did not varied significantly when compared to the first refinement, specifically To was identical and $\varepsilon_{max}^{Flow}/\langle\varepsilon\rangle$ was equal to 271. Smaller value of $\varepsilon_{max}^{Flow}/\langle\varepsilon\rangle$ is caused by less refinement in the impeller region.

Steady state DSD

Since the drop resistance to breakup, ε_{max}, which is used in the formulation of the breakup criteria We_c (Eq. 6), is not known in the studied system *a priori*, we determined its value by the fitting of the calculated mean Sauter drop diameter against the experimental data of Wang and Calabrese.[30] Summary of parameters used in PBE simulation is presented in Table 2. Drop sizes of oils with viscosities ranging from 0.001 to 1 Pa s, which were dispersed in water continuous phase where the interfacial tension was 0.007 N/m and tip speed was 0.94 m/s, were fitted by a unique value of ε_{max}. The agreement with the experimental data was around 8% (Table 3) with the value ε_{max} equal to 32.3 m^2/s^3. This is

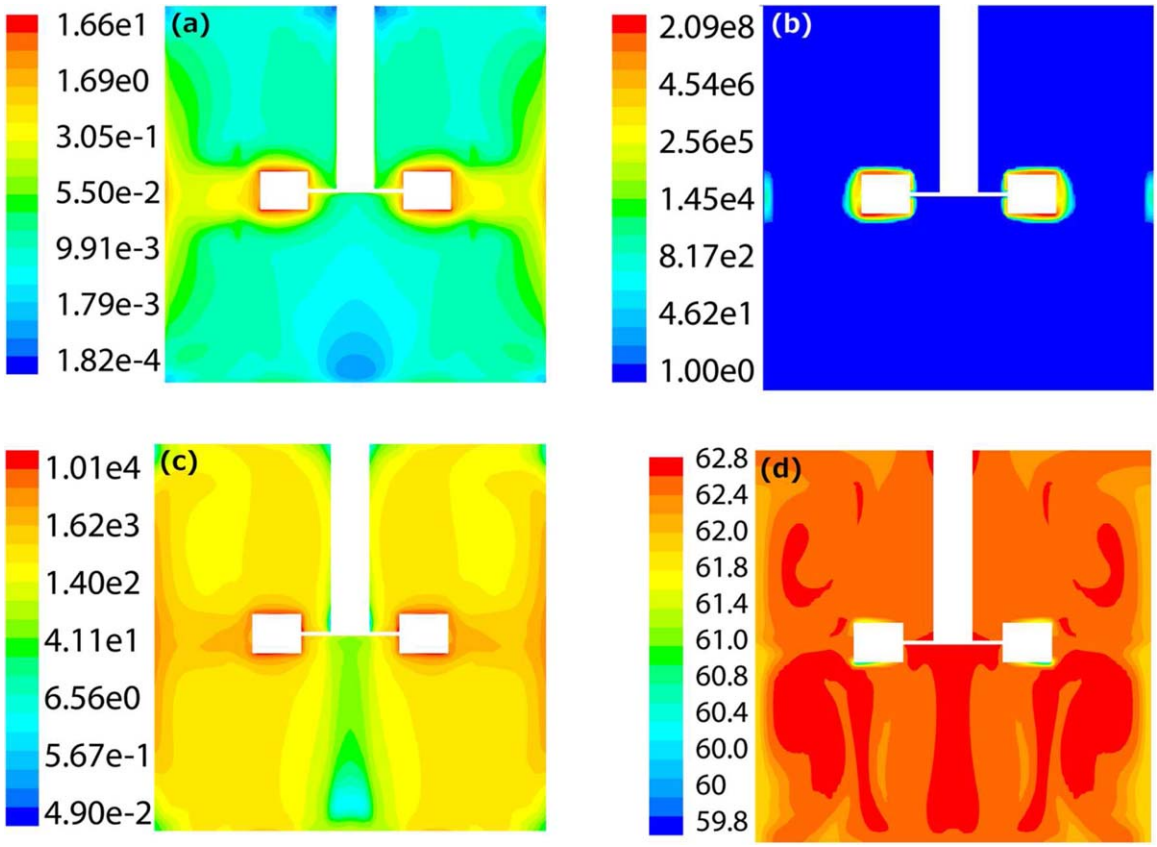

Figure 2. (a) Energy dissipation rate (m^2/s^3) through the tank. High values of ε are present near the impeller and adjacent walls. (b) Breakage birth source term (1/m^{4}s) is near the impeller blades. The region is small but pumping through this region is high.[3,68] (c) Profile of the coalescence birth source term (1/m^{4}s) shows that the coalescence proceeds through the whole tank. Largest intensity is near the impeller where the collision frequency is the highest. Regions directly below impeller and near the tank bends do not support coalescence, possibly due to lack of collisions. (d) Mean Sauter diameter (μm). The drop viscosity was 0.001 Pa s and the interfacial tension was 0.007 N/m.

[Color figure can be viewed in the online issue, which is available at wileyonlinelibrary.com.]

Table 2. Summary of the Model Parameters Used for Simulations

Property	Value	Unit
σ	0.007–0.0378	N/m
η_D	0.001–1	Pa s
η_C	0.0009	Pa s
H_C	0.4×10^{-20}	J
ρ_D	970	kg/m^3
ρ_C	998	kg/m^3
C_4	5	–
λ_{min}	$0.1L_i$	M
λ_{max}	$1L_i$	M

approximately 400 times the vessel averaged value $\langle\varepsilon\rangle$. For comparison, we calculate the mean Sauter drop diameter with ε_{max} equal to $150\cdot\langle\varepsilon\rangle$, which corresponds to the value measured by Zhou and Kresta[1] using Laser Doppler Anemometry in the stirred tank equipped with a Rusthon impeller. The lower value of ε_{max} reduces substantially the size of the formed drops (Table 3) suggesting overestimation of the breakage rate. This indicates that values of ε_{max} measured by the direct methods, that is, by Laser Doppler anemometry[1,34] or velocimetry,[33,69,70] could underestimate the real values present in the system. From another point of view, the studied system was breakage dominant and the measured maximum stable drop size can be used to indirectly determine ε_{max} in the system. Similar concept was used previously by our group[3] where breakup of aggregates composed of polymeric nanoparticles was used to determine ε_{max} present in a stirred tank equipped with a Rushton impeller. Even though a completely different system was used to determine the value of ε_{max}, the obtained ratio of $\varepsilon_{max}/\langle\varepsilon\rangle$ around 550 is rather comparable to our value. Finally, higher values of ε_{max} determined in this study are in agreement with values of ε_{max} calculated from Large Eddy Simulation of the flow generated by the Rushton impeller published previously,[3,36] which provides further validation of the applied methodology.

Once the value of ε_{max} has been determined, it is interesting to compare magnitudes of coalescence and breakup kernels. In Figures 2b, c, there are contour plots of the local source terms describing the drop birth and death, respectively. As can be seen from Figure 2b, the breakage region is limited to the zones with high energy dissipation rates, which are located around the impeller edges and on the adjacent wall. The breakage regions are solely determined by the breakup resistance We_c and the energy dissipation rate present in the mixed vessel. Note that even though the breakage region is rather small, it is also the zone with the highest velocity resulting in a high pumping rate of the fluid.[3]

Table 3. Comparison of the Calculated and Measured Values of the Steady State Mean Sauter Drop Diameter L_{32} Determined for Three Values of the Dispersed-Phase Viscosity and Interfacial Tension of 0.023 N/m

η_D (Pa.s)	L_{32}^{exp} (μm)	$L_{32}^{calc}(*)$ (μm)	Error (*) (%)	$L_{32}^{calc}(**)$ (μm)	Error (**) (%)
0.0008	125	108	14	60	52
0.0834	267	233	13	150	44
0.9919	881	815	8	572	35

$*(\varepsilon_{max}=400\cdot\langle\varepsilon\rangle)$, $**(\varepsilon_{max}=150\cdot\langle\varepsilon\rangle)$

Therefore, even a small zone around the impeller can have a significant impact on the DSD.

Unlike breakage, coalescence is governed by the interplay between the necessary collision frequency (Eq. 18) and sufficient efficiency (Eq. 19). In other words, certain mixing is required for the collision to occur, but the collision should not be too violent for the drops to coalesce (Eq. 24). This is also the reason why, in contrast to breakage source term, the coalescence source term is nonzero in the whole vessel (Figure 2c), although its orders of magnitude is smaller than values of the breakage source term in the breakage zone. This supports that the maximum stable drop size in diluted systems is mainly controlled by the breakup. Numerical experiments without the coalescence terms resulted in a small decrease of the mean Sauter diameters, approximately by 7 % below the original size. The calculations were carried out for viscosities from 0.001 up to 0.1 Pa.s at 180 RPM. Note that other conditions, i.e. higher mixing frequency, may result in more pronounced effect of coalescence.[1]

PBE solved by the QMOM algorithm provides the sizes of three nodes of the DSD which were consequently used to calculate the corresponding Sauter diameter, L_{32}^{local} distributed through the whole vessel (Figure 2d). As expected, the diluted dispersion and small vessel with good mixing results in a homogeneous profile of L_{32}^{local}. To compare the simulations to the values of mean Sauter diameter, L_{32}, measured by Wang and Calabrese[30] and Calabrese et al.[25] L_{32}^{local} was averaged over the whole vessel to obtain L_{32}.

PBE computed on both of the refined meshes resulted in very similar L_{32} as a function of drop viscosities. The calculation of PBE was carried out on the refined mesh with $\sigma=$ 0.015 Nm and 180 rpm. For the ε-based mesh refinement, the resulting L_{32} as a function of drop viscosity exhibited deviance of 1% compared to the original mesh. The PBE calculation on the mesh refined based on velocity gradient resulted in L_{32} approximately 10% higher compared to the calculation with the original mesh. Albeit the small discrepancy, the results agree well with the experimental data. Based on this result, we can conclude that obtained results of the PBE calculation are independent on the used mesh. The original mesh was used in the following simulations of dispersions with variable interfacial tension and mixind speed.

Modelling system with variable interfacial tension

The experimental data and breakup resistance ε_{max} results in a single linear dependency of We_c on the dispersed-phase viscosity (cf. Figure 1), which was obtained for a single interfacial tension, $\sigma=0.007$ Nm. Since We_c contains σ (Eq. 6), a correct master-curve reflects the change in σ. Predictive power of this breakup criteria was tested by predicting the experimental data of Wang and Calabrese,[30] which was measured for σ ranging from $\sigma=0.015-0.0378$ Nm. Since change of interfacial tension was done by mixing various amounts of methanol and water, it was necessary to calculate both flow and consequent PBE. Comparison of the obtained results is presented in Table 4. As can be seen over all the calculated values of L_{32}^{cal} agree very well with measured values with the error not exceeding 25%. The deviation is small and supports the validity of the assumptions used for derivation of the coalescence and breakage kernels as well as shape of DDF. The small differences can be caused by several factors, including not enough time to reach "a true steady state" during the experimental work, imprecision to

Table 4. Comparison of the Mean Sauter Drop Diameter Calculated by Combined CFD-PBE Approach with that Measured Experimentally by Wang and Calabrese[30]

η_D (Pa.s)	L_{32}^{exp} (μm)	L_{32}^{calc} (μm)	Error (%)
$\sigma = 0.0378$ N/m			
0.0010	157	157	0
0.0960	327	308	6
0.4860	671	517	23
0.9710	1017	778	24
$\sigma = 0.023$ N/m			
0.0008	125	108	14
0.0169	158	141	11
0.0834	267	233	13
0.9919	881	815	8
$\sigma = 0.015$ N/m			
0.0008	88	89	1
0.0172	111	113	2
0.0865	180	195	8
0.4080	415	426	3
0.9925	678	578	15
$\sigma = 0.007$ N/m			
0.0008	58	63	8
0.0171	77	81	5
0.0865	138	150	9
0.4153	354	353	1
0.9928	589	559	5

determine the proportionality constant C_5 between Sauter and maximum size, as well as the scatter of the measured values of Sauter mean diameters.

In the formulation of the breakage kernel, there are two parameters which could have a significant impact on formed DSD, that is, the maximum size of eddies which would cause drop breakup λ_{max} and the shape of the DDF expressed by C_4 in Eq. 30.

For η_d equal to 1 Pa s and a tip speed 0.7 m/s, if the value of λ_{max} is increased by factor two, the mean drop size decreases only about 1.3%. This indicates that only eddies of a similar size contribute to breakage significantly which is in accordance with literature.[8,26,45] However, this situation could change with higher ϕ_d, where the equilibrium between breakage and coalescence would be different.

Other parameter, which could have impact on the formed DSD, is the shape of the DDF. Andersson and Andersson[26] studied the breakup of drops with different viscosities and described the resulting change in daughter sizes. We used ternary symmetric breakage as a basis for our computations (C_4 equal to 5).[45] Compared to the binary breakage ($C_4 = 2$), the relative change in L_{32} is only 0.02%. When the mother drop breaks into multiple fragments, which are half of the size of the mother drop, that is, $C_4 = 18$, L_{32} reduces by 10%. Such small effect indicates that simulated results at viscosity $\eta_d = 1$ Pa s are rather insensitive to the choice of the DSD, even though this effect could be more significant for the case of higher ϕ_d or different η_d.

Dependency of mean Sauter diameter on tip speed

With We_c fitting the data of Wang and Calabrese[30] in a range of viscosities and interfacial tensions, we tested the model to predict the drop size measured for a variable tip speed, v_{tip}. Silicone oils with molecular weight, which varied the viscosity from 0.1 to 10 Pa s, were used as the dispersed phase in pure water. The predictions of L_{32}^{cal} at variable v_{tip} and η_d all simulations were carried out with the model parameters defined in Table 2 including the local breakup criterion We_c reported in Figure 1. Investigated range of v_{tip} covered range from 0.4 to 1.2 m/s. Comparison of the obtained results together with experimental data of Calabrese et al.[25] is presented in Figure 3. For completeness we present the data measured by Chen and Middleman,[38] which were obtained in a similar stirred tank with silicon oil with viscosity of 0.001 Pa s. The experimental data show a power-law decrease of the Sauter mean diameter with an increase of the tip speed. Furthermore the size of the maximum stable drop size increases with the increased viscosity of the dispersed phase. For low and moderate dispersed viscosities (0.001–1 Pa s), the power-law dependency L_{32} on tip speed becomes steeper while sudden decrease of the slope is observed for last two highest viscosities. As described by Calabrese et al.,[25] the change in scaling is due to the change in the breakage mechanism, which switches from bursting to elongation or stretching.

The calculated values of L_{32} agree well with the experimental data of Chen and Middleman[38] and Calabrese et al.[25] in the range of low to medium viscosities (0.001–1 Pa s), see Figure 3. Conversely, for the two highest viscosities (5 and 10 Pa s), the model over predicts the measured values of L_{32}. Similar discrepancy was also reported by other authors[29] and can be related to the not-well documented change in the breakup mechanism at higher drop viscosities.[25,26] The sudden change in behavior might be caused by several phenomena including the shear thinning processes, surface instabilities during the drop passage through the high-stress areas, contact with vessel instrumentation, or other

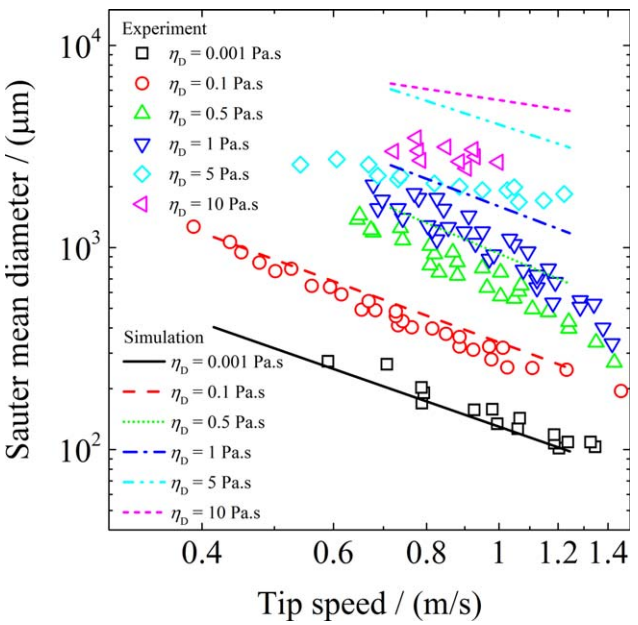

Figure 3. Reproduction of data with variable mixing speed.

Lines represents simulation results while points correspond the experimental data of Calabrese et al.[25] System is composed of pure water with the interfacial tension 0.0378 N/m and oils of variable viscosities. The model captures the drop sizes well for low and moderate viscosities. The absolute values of drop sizes are over-predicted for high viscosities but the change in the scaling is captured by the model. [Color figure can be viewed in the online issue, which is available at wileyonlinelibrary.com.]

mechanism. Note that these mechanisms were not included in the derivation of the breakup kernel.

The shear thinning mechanism was investigated for the case of the highest viscosity 10 Pa s. In particular, we implemented the dependency of used silicone oil viscosity on the shear rate from Dow Chemical database.[71] We assumed the worst case scenario, that is, enough time for the shear thinning effect. The obtained L_{32} did not change significantly from those reported in Figure 3, which indicates a negligible effect of shear thinning.

The significance of the surface instabilities on the breakage of drops was studied by comparison of the characteristic times of the governing processes. These are the relaxation time, which is required to restore the deformed drop to spherical shape by the action of surface forces, and the circulation time, which is required to bring the deformed drop again into the zone with high stresses. The drop relaxation time can be defined as $t_{\mathrm{relax}}=\eta_{\mathrm{d}}L/\sigma$ and it is directly proportional to the dispersed-phase viscosity. Considering the case of a highly viscous polymer in water t_{relax} can rise up to a few seconds. The recirculation time, t_{rec}, in a stirred tank equipped with Rushton impeller[71] was found between 2 and 3 s. This indicates that drop may exhibit amplification of the surface instabilities during multiple passes through the highly turbulent zones, which could result in the enhancement of the breakage usually observed at high viscosities. However, final proof of this hypothesis would require the Lagrangian tracking methods to investigate the stress magnitude along a particle trajectory, which is beyond the scope of the presented work.

Another possible reason for discrepancy between CFD-PBE model, presented in Figure 3, is the change in the flow conditions around a single drop. In particular, by estimating the Stokes number ($St=t_{\mathrm{Char}}\sqrt{\langle\Delta u^2(L)\rangle}/D_{\mathrm{imp}}$ where $t_{\mathrm{Char}}=L^2\rho_{\mathrm{d}}/(18\eta_{\mathrm{c}})$) at places near the impeller, it was found that the Stokes number becomes larger than 1 for drop sizes larger than 2 mm. This indicates that, under experimentally used flow conditions,[25] drops composed of oils with viscosities above 1 Pa s, which form drops larger than 2 mm, might have collided with the vessel instrumentation. The contact could result in higher breakage rate and consequently in smaller drop sizes. Such breakage mechanism was not included in this work and would require substantial modification of the breakage rate expression.

Conclusions

This work deals with the modelling of coalescence and breakup phenomena occurring in a turbulent liquid-liquid dispersion in the fully baffled stirred tank equipped with a Rushton turbine. To capture effect of the local hydrodynamic conditions on the formed drops, we used the combination of CFD and PBE. A breakage criterion was formulated in the form of the local critical Weber number (We_{c}). Experimental data published previously by Wang and Calabrese[30] were used to determine We_{c} as a function of the operating conditions. It was found that We_{c} is independent of the interfacial tension and local energy dissipation rate while it is linearly dependent on the drop viscosity.

In the analyzed vessel, we identified the breakage regions with high energy dissipation rates, which were located in the close vicinity of the impeller. The drop coalescence was observed in the whole vessel, even for a low content of the dispersed phase. Model validation was carried out by experimental data with the variable drop viscosity for a single interfacial tension. Predictions of systems with the variable interfacial tension agree well with the experimental data. Our model also predicts the dependency of Sauter mean diameter on the tip speed reported in Calabrese et al.[25] A very good agreement between the experimental and simulated data was found in region of lower and medium drop viscosities ranging from 0.001 to 1 Pa s. Extrapolation to the higher viscosities correctly predicted the change in the scaling but fails to capture the absolute size of measured drop diameters, which can be explained by the lack of information about the breakup mechanism of highly viscous drops.

The thusly formulated multiscale model of dispersion gives a good starting point for the development of an industrial tool for the design and optimization of the dispersion processes with variable viscosity of the dispersed phase; namely, the suspension, precipitation, and emulsion polymerizations. Currently, our model predictions are limited to the geometries, which are similar to those used in the experimental work, and to low content of the dispersed phase. Further development of the model will address these issues to create a fully predictive tool for an arbitrary geometry and the high content of the dispersed phase. Such tool can be used for optimization, scale-up and design of industrial vessels.

Acknowledgments

The authors are thankful for the support from the Marie Curie Actions (initial training network, Nanopoly PITN-GA-2009-238700), Czech Science Foundation (project GAP106/11/1069) and Specific University Research grant of UCT (number 20/2015). Authors would like to thank Assoc. Prof. Daniele Marchisio (Politecnico di Torino) for suggestions during implementation of QMOM for multiphase flow, and Prof. Massimo Morbidelli and Prof. Giuseppe Storti (ETH Zurich) for many useful discussions. The authors also thank the reviewers for improving this article by insightful comments.

Notations

a_{1-3} = drag coefficient constants, -
B = birth source term, 1/(m^{4}s)
C = arbitrary constant, -
C_1 = hydrodynamic model constant, -
C_2 = hydrodynamic model constant, -
C_3 = statistical velocity constant, -
C_4 = daughter distribution function constant, -
C_5 = ratio between mean and maximum drop size, -
C_η = hydrodynamic model constant, -
C_{D} = drag coefficient, -
d = distance between two points in space, m
D = death source term, 1/(m^{4}s)
D_{imp} = impeller diameter, m
$\mathbf{F}_{drag}$ = drag force, N
$\mathbf{g}$ = gravity acceleration, m/s^2
$g(L)$ = breakage kernel, 1/s
G_{k} = production of the turbulent kinetic energy, kg/(ms^3)
h_{Cr} = critical separation distance, m
h_0 = initial separation distance, m
H = Hamaker constant, J
$h(L_{\mathrm{i}},L_{\mathrm{j}})$ = coalescence kernel, m^3/s
k = turbulent kinetic energy, J/kg
L = drop size, m
N = mixing frequency, 1/s
$n(L_{\mathrm{i}})$ = density function, 1/m^4

p = pressure, Pa
p^B, p^C = breakage and coalescence efficiency, -
R = equivalent radius of collision, m
Re_P = particle Reynolds number, -
St = Stokes number, -
t = time, s
t_{Cr} = critical time necessary for coalescence, s
t_{Co} = coalescence time, s
t_{Char} = characteristics time of flow, s
T = vessel size, m
$\mathbf{T}$ = stress tensor, Pa
$\bar{\mathbf{U}}$ = velocity vector, m/s
u_{Cr}^2 = critical energy of collision, m^2/s^2
Δu^2 = mean square difference in velocity, m^2/s^2
v_{tip} = impeller tip speed, m/s
Vi = viscosity group, -
We_T = tank Weber number, -
y^+ = nondimensional wall distance, -

Greek letters

$\beta(L_i, L_j)$ = daughter distribution function, 1/m
$\dot{\gamma}$ = shear rate, 1/s
ε = energy dissipation rate, m^2/s^3
η_k = Kolmogorov length, m
η_t = turbulent viscosity, Pa s
λ = length of an eddy, m
μ = dynamic viscosity, Pa s
ν = kinematic viscosity, m^2/s
ρ = density, kg/m^3
σ = interfacial tension, N/m
σ_k = hydrodynamic model constant, -
σ_ε = hydrodynamic model constant, -
τ = stress on drop surface, Pa
ϕ = volume fraction, -
$\omega(L, \lambda)$ = coalescence or breakup frequency, 1/s

Subscripts

d = dispersed phase
c = continuous phase
m = mixture of phases
max = maximal value
min = minimal value
i = current drop index
j = other drops indexes
k = index
λ = eddy property

Superscripts

B = breakage
C = coalescence

Literature Cited

1. Zhou GW, Kresta SM. Correlation of mean drop size and minimum drop size with the turbulence energy dissipation and the flow in an agitated tank. *Chem Eng Sci*. 1998;53(11):2063–2079.
2. Hinze JO. Fundamentals of the hydrodynamic mechanism of splitting in dispersion processes. *AIChE J*. 1955;1(3):289–295.
3. Soos M, Kaufmann R, Winteler R, Kroupa M, Luthi B. Determination of maximum turbulent energy dissipation rate generated by a rushton impeller through large eddy simulation. *AIChE J*. 2013; 59(10):3642–3658.
4. Soos M, Ehrl L, Babler MU, Morbidelli M. Aggregate Breakup in a contracting nozzle. *Langmuir*. 2010;26(1):10–18.
5. Harshe YM, Lattuada M, Soos M. Experimental and modeling study of breakage and restructuring of open and dense colloidal aggregates. *Langmuir*. 2011;27(10):5739–5752.
6. Saha D, Soos M, Luthi B, Holzner M, Liberzon A, Babler MU, Kinzelbach W. Experimental characterization of breakage rate of colloidal aggregates in axisymmetric extensional flow. *Langmuir*. 2014;30(48):14385–14395.
7. Venneker BCH, Derksen JJ, Van den Akker HEA. Population balance modeling of aerated stirred vessels based on CFD. *AIChE J*. 2002;48(4):673–685.
8. Laakkonen M, Alopaeus V, Aittamaa J. Validation of bubble breakage, coalescence and mass transfer models for gas-liquid dispersion in agitated vessel. *Chem Eng Sci*. 2006;61(1):218–228.
9. Sungkorn R, Derksen JJ, Khinast JG. Euler-Lagrange modeling of a gas-liquid stirred reactor with consideration of bubble breakage and coalescence. *AIChE J*. 2012;58(5):1356–1370.
10. Azizi F, Al Taweel AM. Turbulently flowing liquid-liquid dispersions. Part I: Drop breakage and coalescence. *Chem Eng J*. 2011; 166(2):715–725.
11. Gimbun J, Rielly CD, Nagy ZK. Modelling of mass transfer in gas-liquid stirred tanks agitated by Rushton turbine and CD-6 impeller: A scale-up study. *Chem Eng Res Des*. 2009;87(4A):437–451.
12. Bannari R, Kerdouss F, Selma B, Bannari A, Proulx P. Three-dimensional mathematical modeling of dispersed two-phase flow using class method of population balance in bubble columns. *Comput Chem Eng*. 2008;32(12):3224–3237.
13. Kerdouss F, Bannari A, Proulx P, Bannari R, Skrga M, Labrecque Y. Two-phase mass transfer coefficient prediction in stirred vessel with a CFD model. *Comput Chem Eng*. 2008;32(8):1943–1955.
14. Montante G, Horn D, Paglianti A. Gas-liquid flow and bubble size distribution in stirred tanks. *Chem Eng Sci*. 2008;63(8):2107–2118.
15. Laakkonen M, Moilanen P, Alopaeus V, Aittamaa J. Modelling local bubble size distributions in agitated vessels. *Chem Eng Sci*. 2007; 62(3):721–740.
16. Wang TF, Wang JF, Jin Y. A CFD-PBM coupled model for gas-liquid flows. *AIChE J*. 2006;52(1):125–140.
17. Chen P, Dudukovic MP, Sanyal J. Three-dimensional simulation of bubble column flows with bubble coalescence and breakup. *AIChE J*. 2005;51(3):696–712.
18. Chen P, Sanyal J, Dudukovic MP. Numerical simulation of bubble columns flows: effect of different breakup and coalescence closures. *Chem Eng Sci*. 2005;60(4):1085–1101.
19. Liao YX, Lucas D. A literature review on mechanisms and models for the coalescence process of fluid particles. *Chem Eng Sci*. 2010; 65(10):2851–2864.
20. Liao YX, Lucas D. A literature review of theoretical models for drop and bubble breakup in turbulent dispersions. *Chem Eng Sci*. 2009;64(15):3389–3406.
21. Pope SB. *Turbulent Flows, 9th print. ed*. Cambridge: Cambridge University Press, 2011.
22. Kolmogorov AN. The local-structure of turbulence in incompressible viscous-fluid for very large Reynolds-numbers. *Proc R Soc Lond Ser A: Math Phys Eng Sci*. 1991;434(1890):9–13.
23. Sreenivasan KR. On the universality of the Kolmogorov constant. *Phys Fluids*. 1995;7(11):2778–2784.
24. Prince MJ, Blanch HW. Bubble coalescence and break-up in air-sparged bubble-columns. *AIChE J*. 1990;36(10):1485–1499.
25. Calabrese RV, Chang TPK, Dang PT. Drop breakup in turbulent stirred-tank contactors. 1. Effect of dispersed-phase viscosity. *AIChE J*. 1986;32(4):657–666.
26. Andersson R, Andersson B. On the breakup of fluid particles in turbulent flows. *AIChE J*. 2006;52(6):2020–2030.
27. Becker PJ, Puel F, Jakobsen HA, Sheibat-Othman N. Development of an improved breakage kernel for high dispersed viscosity phase emulsification. *Chem Eng Sci*. 2014;109:326–338.
28. Luo H, Svendsen HF. Theoretical model for drop and bubble breakup in turbulent dispersions. *AIChE J*. 1996;42(5):1225–1233.
29. Becker PJ, Puel F, Dubbelboer A, Janssen J, Sheibat-Othman N. Coupled population balance-CFD simulation of droplet breakup in a high pressure homogenizer. *Comput Chem Eng*. 2014;68:140–150.
30. Wang CY, Calabrese RV. Drop breakup in turbulent stirred-tank contactors. 2. Relative influence of viscosity and interfacial tension. *AIChE J*. 1986;32(4):667–676.
31. Zhou GW, Kresta SM. Impact of tank geometry on the maximum turbulence energy dissipation rate for impellers. *AIChE J*. 1996; 42(9):2476–2490.
32. Zhou GW, Kresta SM. Evolution of drop size distribution in liquid-liquid dispersions for various impellers. *Chem Eng Sci*. 1998;53(11): 2099–2113.
33. Sharp KV, Adrian RJ. PIV study of small-scale flow structure around a Rushton turbine. *AIChE J*. 2001;47(4):766–778.
34. Ducci A, Yianneskis M. Direct determination of energy dissipation in stirred vessels with two-point LDA. *AIChE J*. 2005;51(8):2133–2149.
35. Derksen J, Van den Akker HEA. Large eddy simulations on the flow driven by a Rushton turbine. *AIChE J*. 1999;45(2):209–221.

36. Micheletti M, Baldi S, Yeoh SL, Ducci A, Papadakis G, Lee KC, Yianneskis M. On spatial and temporal variations and estimates of energy dissipation in stirred reactors. *Chem Eng Res Des*. 2004; 82(A9):1188–1198.
37. Calabrese RV, Wang CY, Bryner NP. Drop breakup in turbulent stirred-tank contactors. 3. Correlations for mean size and drop size distribution. *AIChE J*. 1986;32(4):677–681.
38. Chen HT, Middleman S. Drop size distribution in agitated liquid-liquid systems. *AIChE J*. 1967;13(5):989–995.
39. Rieger R, Weiss C, Wigley G, Bart HJ, Marr R. Investigating the process of liquid-liquid extraction by means of computational fluid dynamics. *Comput Chem Eng*. 1996;20(12):1467–1475.
40. Ghaniyari-Benis S, Hedayat N, Ziyari A, Kazemzadeh M, Shafiee M. Three-dimensional simulation of hydrodynamics in a rotating disc contactor using computational fluid dynamics. *Chem Eng Technol*. 2009;32(1):93–102.
41. Drumm C, Hlawitschka MW, Bart HJ. CFD Simulations and particle image velocimetry measurements in an industrial scale rotating disc contactor. *AIChE J*. 2011;57(1):10–26.
42. Ramkrishna D. *Population Balances: Theory and Applications to Particulate Systems in Engineering*. San Diego, CA: Academic Press, 2000.
43. Fox RO. *Computational Models for Turbulent Reacting Flows*. Cambridge, UK: Cambridge University Press, 2003. .
44. Marchisio DL, Vigil RD, Fox RO. Quadrature method of moments for aggregation-breakage processes. *J Colloid Interface Sci*. 2003; 258(2):322–334.
45. Petitti M, Nasuti A, Marchisio DL, Vanni M, Baldi G, Mancini N, Podenzani F. Bubble size distribution modeling in stirred gas-liquid reactors with QMOM augmented by a new correction algorithm. *AIChE J*. 2010;56(1):36–53.
46. Kennard EH. *Kinetic Theory of Gases, with an Introduction to Statistical Mechanics*, 1st ed. New York, London: McGraw-Hill Book Company, 1938.
47. Jeelani SAK, Hartland S. Effect of interfacial mobility on thin-film drainage. *J Colloid Interface Sci*. 1994;164(2):296–308.
48. Harrats C, Thomas S, Groeninckx G. *Micro- and Nanostructured Polymer Blends: Phase Morphology and Interfaces*. Boca Raton: Taylor & Francis, 2006.
49. Chesters AK. The modeling of coalescence processes in fluid liquid dispersions—a review of current understanding. *Chem Eng Res Des*. 1991;69(4):259–270.
50. Levich VG, Kuznetsov AM. Motion of drops in liquids under influence of surface-active substances. *Doklady Akademii Nauk Sssr*. 1962;146(1):139–183.
51. Andersson R, Andersson B. Modeling the breakup of fluid particles in turbulent flows. *AIChE J*. 2006;52(6):2031–2038.
52. Sprow FB. Distribution of drop sizes produced in turbulent liquid-liquid dispersion. *Chem Eng Sci*. 1967;22(3):435–442.
53. Buffo A, Vanni M, Marchisio DL. Multidimensional population balance model for the simulation of turbulent gas-liquid systems in stirred tank reactors. *Chem Eng Sci*. 2012;70:31–44.
54. Marchisio DL, Fox RO. *Computational Models for Polydisperse Particulate and Multiphase Systems*. Cambridge: Cambridge University Press, 2013.
55. Bird RB, Stewart WE, Lightfoot EN. *Transport Phenomena*, *2nd ed.* New York: Wiley, 2002.
56. Ishii M, Zuber N. Drag coefficient and relative velocity in bubbly, droplet or particulate flows. *AIChE J*. 1979;25(5):843–855.
57. Hayashi K, Tomiyama A. A drag correlation of fluid particles rising through stagnant liquids in vertical pipes at intermediate Reynolds numbers. *Chem Eng Sci*. 2009;64(12):3019–3028.
58. Morsi SA, Alexander AJ. Investigation of particle trajectories in 2-phase flow systems. *J Fluid Mech*. 1972;55:193–208.
59. Gordon RG. Error bounds in equilibrium statistical mechanics. *J Math Phys*. 1968;9(5):655–663.
60. Press WH. *Numerical Recipes in C: The Art of Scientific Computing*, *2nd ed*. Cambridge: Cambridge University Press, 1992.
61. Rutherford K, Mahmoudi SMS, Lee KC, Yianneskis M. The influence of Rushton impeller blade and disk thickness on the mixing characteristics of stirred vessels. *Chem Eng Res Des*. 1996;74(A3):369–378.
62. Joshi JB, Nere NK, Rane CV, Murthy BN, Mathpati CS, Patwardhan AW, Ranade VV. CFD simulation of stirred tanks: comparison of turbulence models. Part I: radial flow impellers. *Can J Chem Eng*. 2011;89(1):23–82.
63. Rushton JH, Costich EW, Everett HJ. Power characteristics of mixing impellers. 1. *Chem Eng Prog*. 1950;46(8):395–404.
64. Rushton JH, Costich EW, Everett HJ. Power characteristics of mixing impellers. 2. *Chem Eng Prog*. 1950;46(9):467–476.
65. Distelhoff MFW, Laker J, Marquis AJ, Nouri JM. The application of a strain-gauge technique to the measurement of the power characteristics of 5 impellers. *Exp Fluids*. 1995;20(1):56–58.
66. Sahu AK, Kumar P, Joshi JB. Simulation of flow in stirred vessel with axial flow impeller: Zonal modeling and optimization of parameters. *Ind Eng Chem Res*. 1998;37(6):2116–2130.
67. Nere NK, Patwardhan AW, Joshi JB. Liquid-phase mixing in stirred vessels: Turbulent flow regime. *Ind Eng Chem Res*. 2003;42(12): 2661–2698.
68. Nienow AW. On impeller circulation and mixing effectiveness in the turbulent flow regime. *Chem Eng Sci*. 1997;52(15):2557–2565.
69. Escudie R, Line A. Experimental analysis of hydrodynamics in a radially agitated tank. *AIChE J*. 2003;49(3):585–603.
70. Baldi S, Ducci A, Yianneskis M. Determination of dissipation rate direct measurement of fluctuating in stirred vessels through velocity gradients. *Chem Eng Technol*. 2004;27(3):275–281.
71. DowChemicals. Available at: http://www.dowcorning.com/content/discover/discoverchem/weight-vs-viscosity.aspx. Accessed on December 9, 2014.
72. Kalal Z, Jahoda M, Fort I. CFD prediction of gas-liquid flow in an aerated stirred vessel using the population balance model. *Chem Process Eng-Inz*. 2014;35(1):55–73.
73. Paul EL, Atiemo-Obeng VA, Kresta SM. *Handbook of Industrial Mixing: Science and Practice*. Hoboken, NJ: Wiley-Interscience, 2004.

Manuscript received Dec. 29, 2014, and revision received Mar. 11, 2015.